

Thermal transport in composition graded silicene/germanene heterostructures

Zengqiang Cao(曹增强), Chaoyu Wang(王超宇), Honggang Zhang(张宏岗), Bo You(游波), and Yuxiang Ni(倪宇翔)

Citation: Chin. Phys. B, 2024, 33 (**4**): 044402. DOI: 10.1088/1674-1056/ad1500
Journal homepage: http://cpb.iphy.ac.cn; http://iopscience.iop.org/cpb

What follows is a list of articles you may be interested in

Influences of double diffusion upon radiative flow of thin film Maxwell fluid through a stretching channel

Arshad Khan, Ishtiaq Ali, Musawa Yahya Almusawa, Taza Gul, and Wajdi Alghamdi
Chin. Phys. B, 2023, 32 (**8**): 084401. DOI: 10.1088/1674-1056/acc059

Thermal rectification induced by Wenzel-Cassie wetting state transition on nano-structured solid-liquid interfaces

Haiyang Li(李海洋), Jun Wang(王军), and Guodong Xia(夏国栋)
Chin. Phys. B, 2023, 32 (**5**): 054401. DOI: 10.1088/1674-1056/aca9c1

Construction and mechanism analysis on nanoscale thermal cloak by *in-situ* annealing silicon carbide film

Jian Zhang(张健), Hao-Chun Zhang(张昊春), Zi-Liang Huang(黄子亮), Wen-Bo Sun(孙文博), and Yi-Yi Li(李依依)
Chin. Phys. B, 2022, 31 (**1**): 014402. DOI: 10.1088/1674-1056/ac2809

Uniformity principle of temperature difference field in heat transfer optimization

Xue-Tao Cheng(程雪涛), Xin-Gang Liang(梁新刚)
Chin. Phys. B, 2019, 28 (**6**): 064402. DOI: 10.1088/1674-1056/28/6/064402

Three-dimensional human thermoregulation model based on pulsatile blood flow and heating mechanism

Si-Na Dang(党思娜), Hong-Jun Xue(薛红军), Xiao-Yan Zhang(张晓燕), Jue Qu(瞿珏), Cheng-Wen Zhong(钟诚文), Si-Yu Chen(陈思宇)
Chin. Phys. B, 2018, 27 (**11**): 114402. DOI: 10.1088/1674-1056/27/11/114402

SPECIAL TOPIC — Heat conduction and its related interdisciplinary areas

Thermal transport in composition graded silicene/germanene heterostructures

Zengqiang Cao(曹增强)[1,†], Chaoyu Wang(王超宇)[2,†], Honggang Zhang(张宏岗)[3], Bo You(游波)[2], and Yuxiang Ni(倪宇翔)[1,‡]

[1] *School of Physical Science and Technology, Southwest Jiaotong University, Chengdu* 610031, *China*

[2] *Department of Materials Science and the Advanced Coatings Research Center of the China Educational Ministry, Fudan University, Shanghai* 200433, *China*

[3] *Key Laboratory of High Performance Scientific Computation, School of Science, Xihua University, Chengdu* 610039, *China*

(Received 31 October 2023; revised manuscript received 27 November 2023; accepted manuscript online 13 December 2023)

Through equilibrium and non-equilibrium molecular dynamics simulations, we have demonstrated the inhibitory effect of composition graded interface on thermal transport behavior in lateral heterostructures. Specifically, we investigated the influence of composition gradient length and heterogeneous particles at the silicene/germanene (SIL/GER) heterostructure interface on heat conduction. Our results indicate that composition graded interface at the interface diminishes the thermal conductivity of the heterostructure, with a further reduction observed as the length increases, while the effect of the heterogeneous particles can be considered negligible. To unveil the influence of composition graded interface on thermal transport, we conducted phonon analysis and identified the presence of phonon localization within the interface composition graded region. Through these analyses, we have determined that the decrease in thermal conductivity is correlated with phonon localization within the heterostructure, where a stronger degree of phonon localization signifies poorer thermal conductivity in the material. Our research findings not only contribute to understanding the impact of interface gradient-induced phonon localization on thermal transport but also offer insights into the modulation of thermal conductivity in heterostructures.

Keywords: composition graded interface, thermal transport, phonon localization, molecular dynamics

PACS: 44.90.+c, 02.70.Ns, 74.78.Fk, 29.50.+v **DOI:** 10.1088/1674-1056/ad1500

1. Introduction

Based on the hexagonal honeycomb structure of graphene, many novel two-dimensional (2D) materials such as silicene, stanene, phosphorene, and transition-metal dichalcogenides (TMDs) have been successfully synthesized, showcasing excellent electrical, thermal, and mechanical properties.[1–7] To meet the demands of various nanoscale devices, the unique properties exhibited by heterostructures composed of different monolayers have garnered significant attention. These distinct two-dimensional materials seamlessly combine two different atomic monolayers within a two-dimensional plane through covalent bonding, forming in-plane heterostructures.[8] In comparison to vertical heterostructures, these in-plane heterostructures offer more easily controllable integration and superior heat transfer pathways, demonstrating immense potential in the development of novel micro-/nanoelectronic devices.[9]

In recent years, with the increasingly mature synthesis techniques for 2D lateral heterostructures, various novel two-dimensional lateral heterostructures have been reported.[10] However, compositional transition at the interfaces of 2D heterostructures has remained a challenge, making the fabrication of clean and well-defined interfaces a persistent issue. The synthesis and pattern-recognition technique proposed by Levendorf *et al.*[11] has successfully prepared graphene and h-BN (Gr/h-BN) in-plane heterostructures. Multiple studies indicate the presence of atomic intermixing at the lateral interface of Gr/h-BN, with atomic intermixing extending over a width of no more than 10 nm. Gong *et al.*[12] reported a single-step vapor phase growth process, demonstrating the growth of lateral WS_2/MoS_2 heterostructures with sharp interfaces. Ogikubo *et al.*[13] utilized a synergistic growth approach involving atomic segregation epitaxy (ASE) and molecular beam epitaxy (MBE) to fabricate lateral monolayer heterostructures of germanene/stanene on Ag(111) thin films. Using scanning tunneling microscopy (STM), they observed domain boundaries with armchair and zigzag edge structures at the interface.

In contrast to earlier two-dimensional materials like silicene, which could only be synthesized on metal substrates such as Ag, ZrB_2, and Lr, recent work by Quertite *et al.*[14] has confirmed the successful preparation of silicene nanoribbons on insulating NaCl thin films. This significant breakthrough has paved the way for a new approach to the synthesis of novel two-dimensional materials. Considering the compatibility of silicene with existing silicon-based electronics industry,[15–17] SIL/GER nanoribbons hold a broader application potential

†These authors contributed equally to this work.

‡Corresponding author. E-mail: yuxiang.ni@swjtu.edu.cn

© 2024 Chinese Physical Society and IOP Publishing Ltd

in nanoelectronic devices. Yang *et al*. calculated based on density functional theory that the thermal electric *ZT* values for SIL/GER superlattices and disordered SIL/GER nanoribbons are twice as high as those of individual materials.[18] The excellent electrical properties and low thermal conductivity bestow SIL/GER heterostructures with significant potential as thermoelectric materials. While the thermal conductivity of SIL/GER superlattice structures has been extensively investigated,[19] the relationship between the presence of interface composition diffusion, especially in SIL/GER lateral heterostructures, and their thermal conductivity, particularly concerning experimentally observed structures, remains unclear. In this article, we employ molecular dynamics simulations to explore the influence of different interface composition-graded models on the thermal conductivity. We also employ phonon analysis to elucidate the underlying physical mechanisms.

2. Method

2.1. Models

To begin with, for model construction, a SIL/GER lateral heterostructure with dimensions of 5.1×50.4 nm^2 was selected to investigate the thermal transport behavior induced by interface atomic transition. To minimize the influence of lattice mismatch on the thermal performance calculations of the heterostructure, the lattice constants for SIL and GER were set to 3.83 Å and 3.97 Å, respectively, while the initial buckling heights for SIL and GER were set to 0.44 Å and 0.64 Å, respectively.[20] According to Fick's law[21] ($J=-D(\partial\rho/\partial x)$, where J is the diffusion flux, D is the diffusion coefficient, ρ is the mass concentration, and x is the diffusion distance), it is understood that the number of heterogeneous particles at the interface is inversely related to the composition transition length (L). To construct a realistic non-abrupt interface composition-graded model, we introduced randomness in the interface atomic transition and allowed the number of diffusing atoms to decrease with increasing transition distance. We constrained the maximum number of diffusing atoms at the interface to be half of the total number of atoms. For the interface composition-graded model, we conducted random atomic transition with a fixed transition concentration to explore the relationship between the composition gradient length and thermal transport behavior.

As depicted in Fig. 1(a), we have established five interface models with varying transition lengths, i.e., 0 nm (abrupt interface), 8 nm, 16 nm, 24 nm, and 32 nm. The atomic ratio of Si to Ge, as depicted on both sides of the abrupt interface (highlighted by the red dashed line), is set at 1:1. Furthermore, as shown in Fig. 1(b), models incorporating heterogeneous particles composed of different numbers of atoms (including 1 atom, 2 atoms, 4 atoms, and 6 atoms) have been constructed to closely approximate actual interface models. It is important to note that the transition mechanism and process remain consistent with those of single atom composition-graded models, with the distinction lying in the nature of the heterogeneous particles.

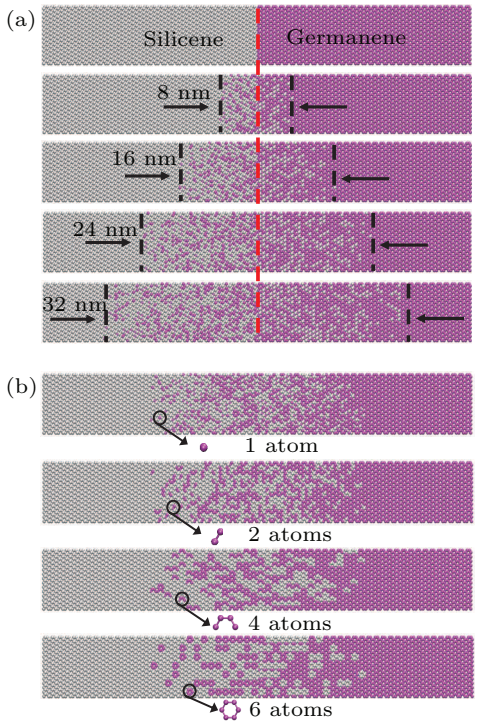


Fig. 1. (a) Structures of SIL/GER lateral heterostructure with abrupt interface and composition transition interfaces with different lengths. (b) Model illustrations depicting six distinct heterogeneous particles with varying atom counts.

2.2. EMD method for κ_x and NEMD for $R_{\rm int}$

Molecular dynamics (MD) simulations have gained widespread usage due to their ability to accurately describe interfacial heat transfer at the atomic scale. In this study, both equilibrium molecular dynamics (EMD) and non-equilibrium molecular dynamics (NEMD) simulation methods were employed to investigate the thermal conductivity and interfacial thermal resistance of SIL/GER heterostructures with diffusive interfaces. It has been reported that the Stillinger–Weber (SW) potential effectively describes the bending structures and thermophysical properties of SIL and GER.[19,22–24] In this paper, the Si–Si, Ge–Ge, and Si–Ge interactions within SIL/GER nanoribbons were characterized using the SW potential,[25,26] with the Si–Ge interaction based on the mixing rules described.[27] To eliminate boundary effects and simulate independent structures, periodic boundary conditions were applied in three directions based on the models in Fig. 1, and a 10 nm vacuum layer was added in the direction perpendicular to the plane. The MD time step was set to 0.5 fs. Initially, a conjugate gradient (CG) energy minimization algorithm was employed to relieve internal stresses within the heterostructure and find the minimum energy state. Subsequently,

the structure was relaxed under the NVT ensemble at a fixed temperature of 300 K for 500 ps to stabilize the structure. Finally, a 300 ps dynamic equilibrium in the microcanonical ensemble (NVE) was performed to achieve complete structural relaxation.

To compute the thermal conductivity (κ_x) along the transition plane direction (along the x-axis), we collected instantaneous heat flux, denoted as $j_x(t)$, during a 2 ns time period while running under the NVE ensemble. The thermal conductivity κ_x was then calculated using the Green–Kubo formula[28]

$$\kappa_x = \frac{V}{k_B T^2}\int_0^{+\infty}\langle j_x(t) j_x(0)\rangle \,\mathrm{d}t. \tag{1}$$

Here, k_B represents the Boltzmann constant, T denotes the temperature, and V stands for the volume. Angle brackets indicate ensemble averages, which were obtained by averaging results from twenty independent MD simulations.

To compute the interfacial thermal resistance (R_{int}) at the heterostructure interface using the NEMD method, we initially designated heat sources and heat sinks at the left and right ends of the model while immobilizing the edges at both ends. The intermediate portion, excluding the heat baths and the fixed regions, was partitioned to establish a temperature gradient. Subsequently, under the NVE ensemble, we collected the average temperatures for each component in the middle part of the model, along with the energy exchange between the heat source and the heat sink. Relying on Fourier's law, we calculated the total thermal resistance "R_{tot}" of the material. For non-abrupt interface composition-graded models, where the heterostructure's interface is not precisely defined, we regarded R_{int} as the interfacial thermal resistance of the SIL/GER lateral heterostructure. The specific calculation formula is as follows:

$$R_{tot} = \frac{A}{l_{SIL}\cdot\kappa_{SIL}} + R_{int} + \frac{A}{l_{GER}\cdot\kappa_{GER}}. \tag{2}$$

In the equation, κ_{SIL} (κ_{GER}) represents the thermal conductivity of the corresponding SIL (GER) portion within the heterostructure. l_{SIL} (l_{GER}) signifies the length of the SIL (GER) in the heterostructure. The cross-sectional area (A) was determined based on a SIL thickness of 4.2 Å.[29] It is noteworthy that, based on the linear portion of the temperature gradient obtained using the NEMD method, we calculated the thermal conductivity of SIL and GER through Fourier's law.

2.3. Phonon transmission calculations

Phonons, also referred to as quanta of lattice vibrations, serve as the primary heat carriers in semiconductor materials, and they determine a material's thermal conductivity. We employed three phonon analysis methods: phonon transmission coefficient, phonon localization length, and phonon participation rate to investigate the underlying physical mechanisms of the impact of compositional transition on heat transfer in SIL/GER heterostructures. The phonon transmission coefficient quantifies the phonon transport capability within a material, specifically the ability to transfer thermal energy in the presence of resistance along a particular direction. Following the NEMD method proposed by K. Saaskilahti *et al.*,[30,31] we computed the phonon transmission function ($T(w)$) to quantify the impact of phonon scattering on heat energy transfer. Initially, the frequency-resolved heat flux $q_{i\to j}(w)$ between any arbitrary atoms i and j can be calculated by

$$q_{i\to j}(w) \approx -\frac{2}{t_{simu}\omega} \times \sum_{\alpha,\beta\in\{x,y,z\}} \mathrm{Im}\left\langle \hat{v}_i^{\alpha}(\omega) K_{ij}^{\alpha\beta} \hat{v}_j^{\beta}(\omega)\right\rangle, \tag{3}$$

$$q(w) = \sum_{i\in L}\sum_{j\in R} q_{i\to j}(\omega), \tag{4}$$

$$T(w) = \frac{q(w)}{k_B \Delta T}. \tag{5}$$

Here, t_{simu} denotes the simulation time, ω represents the frequency, and $\hat{v}_i^{\alpha}(\omega)$ and $\hat{v}_j^{\beta}(\omega)$ correspond to the Fourier-transformed atomic velocities of atom i in direction α and atom j in direction β, respectively. Subsequently, the heat flow across the interface is obtained based on Eq. (4), where L and R denote the separation sets of any adjacent atoms at the interface. Finally, the phonon transmission coefficient $T(w)$ through the interface is computed using Eq. (5), with k_B representing the Boltzmann constant and ΔT indicating the temperature difference between the two ends of the heat bath. Since Fourier transformation involves converting time-domain statistics into frequency-domain analysis, the abscissa of the resulting transmission coefficient plots is expressed in THz for frequency, while the ordinate represents the magnitude of the transmission coefficient.

3. Results and discussion

3.1. Thermal conductivity and interface thermal resistance of SIL/GER lateral heterostructures

The computed temperature gradients for the structures in Fig. 1 are depicted in Fig. 2. Panels (a), (b), (c), and (d) represent the temperature gradient profiles for transition lengths of 0 nm (abrupt interface), 8 nm, 16 nm, and 24 nm, respectively. Note that the temperature gradient for 32 nm is not shown here as it is nearly identical to that of 24 nm. As observed in Fig. 2(a), a significant temperature discontinuity is evident at the interface. In contrast, for the atomic transition interfaces described in Figs. 2(b)–2(d), the temperature at the interface transitions from a discontinuity to a smooth decrease, and the temperature gradient in this region becomes more gradual as the transition length increases. This transition is primarily attributed to the introduction of the composition-graded inter-

face, which reduces the difference in atomic species at the interface. Considering that phonons, as the primary heat carriers in semiconductors, experience significant interface scattering, leading to substantial interfacial thermal resistance when propagating as waves to the SIL/GER interface.

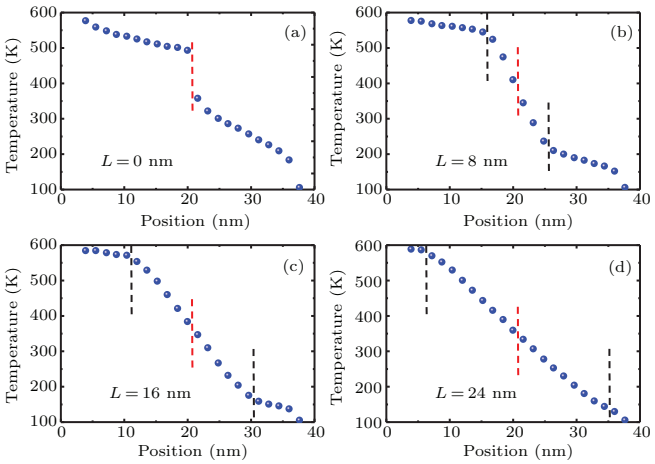


Fig. 2. Illustrates the temperature gradients corresponding to different compositional transition lengths with 1 atom heterogeneous particle: (a) 0 nm, (b) 8 nm, (c) 16 nm, and (d) 24 nm.

Table 1. The R_{int} with abrupt interface $L = 0$ nm and different component transition lengths.

L (nm)	0	8	16	24	32
R_{int} (10^{-9} m^2·K/W)	3.17	5.04	6.95	8.67	9.21

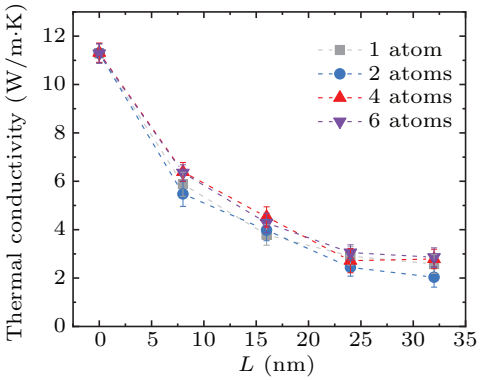


Fig. 3. The thermal conductivity at various compositional transition lengths: 0 nm (abrupt interface), 8 nm, 16 nm, 24 nm, and 32 nm.

As shown in Table 1, we computed the R_{int} based on the simulated temperature profiles presented in Fig. 2 using Eq. (2). From the table, it is evident that the introduction of the transition interface results in a greater thermal resistance, with R_{int} increasing as the transition length grows. We also calculated R_{int} for different elemental transition models with $L = 16$ nm, as shown in Table 2. We found that R_{int} related to component transitions is insensitive to non-uniform particle sizes. To validate this result, we computed the thermal conductivity of the SIL/GER lateral heterostructure using the EMD method. As depicted in Fig. 3, with an increase in interface transition length, the material's thermal conductivity gradually decreases. Furthermore, as the transition length increases, the influence of heterogeneous particles on the thermal conductivity becomes less pronounced. This outcome is consistent with the results obtained from the calculations of R_{int} in Table 2.

Table 2. The R_{int} for various heterogeneous particles composed of different numbers of atoms (n) at a component transition length (L) of 16 nm.

n	1	2	4	6
R_{int} (10^{-9} m^2·K/W)	6.95	7.41	6.30	6.35

3.2. Phonon analysis and Anderson localization in SIL/GER lateral heterostructures

To explore the underlying mechanisms of how the interface transition length affects thermal transport in SIL/GER, we conducted phonon analysis on the heterostructure. As described in the previous section regarding phonon transmission function calculations, in Fig. 4(a), we compared the phonon transmission coefficients of pure silicene and germanene with those of the abrupt interface and graded interface. From the graph, it's evident that SIL exhibits a wider frequency-domain transmission coefficient compared to GER, and, for the most part, SIL surpasses GER within a wide frequency range. This result also explains why SIL has a higher thermal conductivity than GER. Furthermore, it can be observed from the figure that, with an increase in the transition length L, the material's transmission coefficient decreases, corresponding to the decrease in the material's thermal conductivity with the increasing L. Finally, we also noted that the cutoff frequency for the transmission coefficient of the heterogeneous structure is approximately 12 THz, which is consistent with the cutoff frequency of GER. This indicates that the cutoff frequency of the transmission coefficient in heterogeneous structures with interfaces is essentially the same as the lower cutoff frequency in the two individual materials. As shown in Figs. 4(b) and 4(c), for further investigation into the influence of the heterogeneous particles on thermal transport in the heterogeneous structure, we separately computed the phonon transmission functions for heterogeneous particles consisting of 1 atom and 4 atoms. In both cases, the transmission coefficient decreases with an increase in transition length, ultimately converging. This result aligns well with the trend of thermal conductivity, which decreases with an increase in transition length and approaches a plateau. Moreover, based on the calculations of the transmission coefficients and thermal conductivity for the heterogeneous structure, we can see that the variations between the abrupt interface and graded interface are more significant and pronounced compared to the differences between graded interface and graded interface. This may be attributed to the increased disorder in the system caused by the interfacial transition of components, leading to phonon localization, thereby impeding the transfer of thermal energy.[32,33]

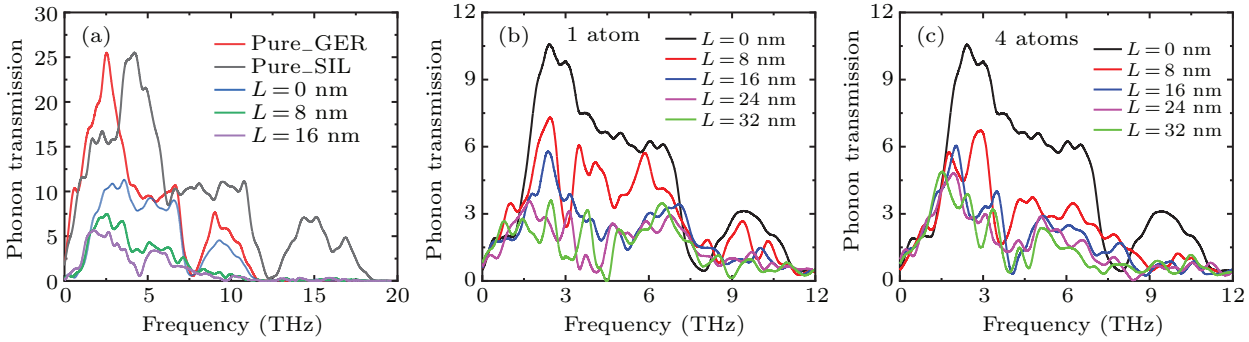


Fig. 4. (a) The phonon transmission coefficients of SIL, GER and SIL/GER with different L. The phonon transmission coefficients of different heterogeneous particles (b) 1 atom and (c) 4 atoms at different L.

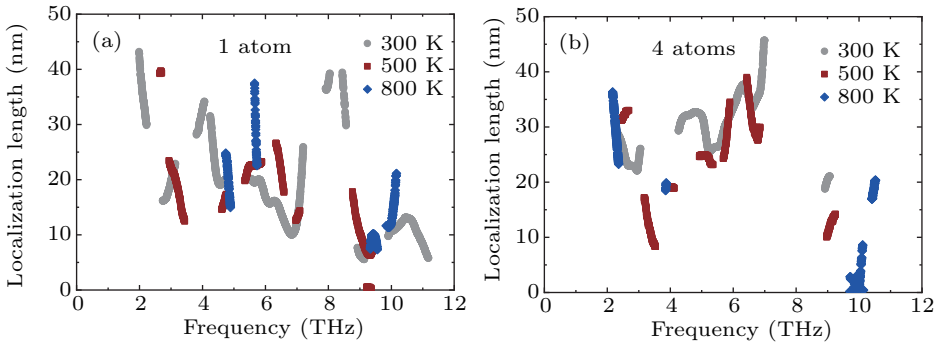


Fig. 5. Phonon localization length of different heterogeneous particles at different temperatures.

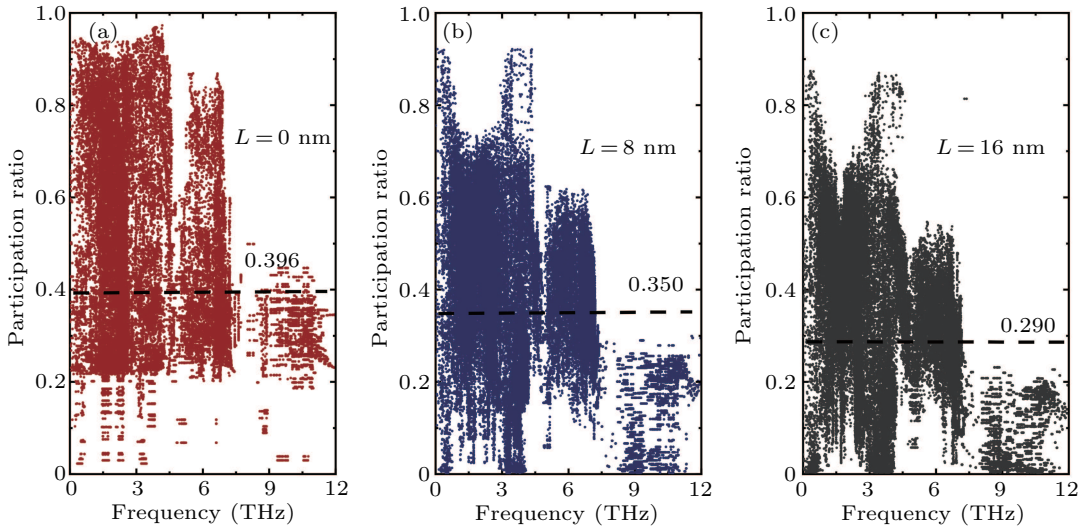


Fig. 6. A comparison of the phonon participation rates in SIL/GER lateral heterostructures with different L. The black dashed line represents the mean value.

According to Anderson localization theory,[34,35] when phonons propagate in heterogeneous structures, they may exhibit phonon localization phenomena, including back-and-forth phonon reflections and the formation of localized phonon standing waves. In recent years, researchers have extensively focused on the impact of phonon localization on the thermal conductivity of nanostructures.[36–39] To investigate the relationship between phonon localization phenomena, temperature, and the heterogeneous particles, we calculated the phonon localization length (ξ) in the SIL/GER heterogeneous structure, which can be expressed as

$$T(\omega) = T_0(\omega) \cdot \mathrm{e}^{-L/\xi}, \tag{6}$$

where L is the length of the graded interface, $T_0(\omega)$ is the phonon transmission coefficient when $L = 0$ nm (abrupt interface), and $T(\omega)$ is the respective phonon transmission coefficient for various graded interface lengths. Due to inherent computational errors, our model and data cannot perfectly fit. We introduced the parameter R^2, ranging from 0 to 1, to assess the goodness of fit of the parameters.[40] A larger R^2 value indicates a better fit, signifying a stronger correlation between the model and the data.

As shown in Fig. 5, the calculated phonon localization results were obtained under the condition of $R^2 > 0.95$. Figures 5(a) and 5(b) represent the phonon localization lengths at various frequencies for heterogeneous particles of 1 atom and 4 atoms at temperatures of 300 K, 500 K, and 800 K, respectively. From these two figures, it is evident that phonon localization primarily occurs in the mid-to-low frequency range, and the extent of phonon localization decreases as the temperature rises. To quantitatively assess the impact of phonon localization,[41] Fig. 6 illustrates the phonon participation ratio for the heterogeneous structure with different graded interface lengths (0 nm, 8 nm, and 16 nm). The results demonstrate that, with an increasing graded interface length, the proportion of phonons with a participation ratio less than 0.1 increases, and the average phonon participation ratio gradually decreases. This corresponds to a more pronounced degree of phonon localization with increasing graded interface length, providing a clear explanation for the decrease in thermal conductivity in SIL/GER heterostructures as the interface transition length increases.

4. Conclusion

In summary, through molecular dynamics simulations, we have demonstrated that interfaces with heterogeneous particles can effectively suppress the thermal conductivity of lateral heterostructures in the case of SIL/GER. Specifically, we have observed that as the compositional transition length increases, the thermal conductivity gradually decreases and approaches a plateau. Our analysis indicates that, in contrast to abrupt heterostructure interfaces, heterostructures with graded interfaces exhibit phonon localization during the phonon transmission process, and increasing the transition length exacerbates this phenomenon. This fundamental insight provides guidance on how to control lateral heterostructures to reduce their thermal performance.

Acknowledgement

Project supported by the National Natural Science Foundation of China (Grant No. 12104291).

References

[1] Bhimanapati G R, Lin Z, Meunier V, *et al*. 2015 *ACS Nano* **9** 11509
[2] Tan C, Cao X, Wu X J, *et al*. 2017 *Chem. Rev.* **117** 6225
[3] Wang L, Hu P, Long Y, *et al*. 2017 *J. Mater. Chem. A* **5** 22855
[4] Khan K, Tareen A K, Aslam M, *et al*. 2020 *J. Mater. Chem. C* **8** 387
[5] Butler S Z, Hollen S M, Cao L, *et al*. 2013 *ACS Nano* **7** 2898
[6] Zhu F F, Chen W J, Xu Y, *et al*. 2015 *Nat. Mater.* **14** 1020
[7] Balendhran S, Walia S, Nili H, *et al*. 2015 *Small* **11** 640
[8] Ling X, Lin Y, Ma Q *et al*. 2015 arXiv preprint arXiv:1512.04492
[9] Jia L, Wu J, Zhang Y, *et al*. 2022 *Small Methods* **6** 2101435
[10] Wang J, Li Z, Chen H, *et al*. 2019 *Nano-Micro Lett.* **11** 48
[11] Levendorf M P, Kim C J, Brown L, *et al*. 2012 *Nature* **488** 627
[12] Gong Y, Lin J, Wang X, *et al*. 2014 *Nat. Mater.* **13** 1135
[13] Ogikubo T, Shimazu H, Fujii Y, *et al*. 2020 *Adv. Mater. Interfaces* **7** 1902132
[14] Quertite K, Enriquez H, Trcera N, *et al*. 2021 *Adv. Funct. Mater.* **31** 2007013
[15] Zhao J, Liu H, Yu Z, *et al*. 2016 *Prog. Mater. Sci.* **83** 24
[16] Kara A, Enriquez H, Seitsonen A P, *et al*. 2012 *Surf. Sci. Rep.* **67** 1
[17] Vogt P, De Padova P, Quaresima C, *et al*. 2012 *Phys. Rev. Lett.* **108** 155501
[18] Yang K, Cahangirov S, Cantarero A, *et al*. 2014 *Phys. Rev. B* **89** 125403
[19] Wang X, Hong Y, Chan P K, *et al*. 2017 *Nanotechnology* **28** 255403
[20] Cahangirov S, Topsakal M, Aktürk E, *et al*. 2009 *Phys. Rev. Lett.* **102** 236804
[21] Brogioli D and Vailati A 2000 *Phys. Rev. E* **63** 012105
[22] Liu B, Baimova J A, Reddy C D, *et al*. 2014 *ACS Appl. Mater. Interfaces* **6** 18180
[23] Liu B, Baimova J A, Reddy C D, *et al*. 2014 *Carbon* **79** 236
[24] Zhou Y, Zhang X and Hu M 2015 *Phys. Rev. B* **92** 195204
[25] Zhang X, Xie H, Hu M, *et al*. 2014 *Phys. Rev. B* **89** 054310
[26] Ding K and Andersen H C 1986 *Phys. Rev. B* **34** 6987
[27] Ethier S and Lewis L J 1992 *J. Mater. Res.* **7** 2817
[28] Kubo R, Toda M and Hashitsume N 1991 *Statistical Physics II: Nonequilibrium Statistical Mechanics* (Springer-Verlag)
[29] Hu M, Zhang X and Poulikakos D 2013 *Phys. Rev. B* **87** 195417
[30] Sääskilahti K, Oksanen J, Tulkki J, *et al*. 2014 *Phys. Rev. B* **90** 134312
[31] Sääskilahti K, Oksanen J, Volz S, *et al*. 2015 *Phys. Rev. B* **91** 115426
[32] Ni Y, Zhang H, Hu S, *et al*. 2019 *Int. J. Heat Mass Transf.* **144** 118608
[33] Ni Y and Volz S 2021 *J. Appl. Phys.* **130** 190901
[34] Anderson P W 1958 *Phys. Rev* **109** 1492
[35] Lee P A and Fisher D S 1981 *Phys. Rev. Lett.* **47** 882
[36] Zhang W, Guo Y, Xiong S Y, *et al*. 2023 *Phys. Rev. B* **108** 125436
[37] Liu Y, Yue J, Liu Y, *et al*. 2023 *Chin. Phys. Lett.* **40** 086301
[38] Nomura M, Anufriev R, Zhang Z, *et al*. 2022 *Mater. Today Phys.* **22** 100613
[39] Ma D, Li X and Zhang L 2020 *Chin. Phys. B* **29** 126502
[40] Nagelkerke N J 1991 *Biometrika* **78** 691
[41] Monthus C and Garel T 2010 *Phys. Rev. B* **81** 224208